Deformation-Mode-Dependent Transient Response of Continuous-Facesheet MEMS Deformable Mirrors

Dhruv Lakhani | Joseph Boales | Steven Cornelissen

INTRODUCTION

Adaptive optics systems require deformable mirrors capable of rapidly generating accurate wavefronts over a wide range of aberration shapes and characteristics. Advances in wavefront sensing, high-speed imaging, and real-time control have increased the contribution of the dynamic response of the deformable mirror to overall system performance. Continuous-facesheet MEMS deformable mirrors are widely used because they provide high actuator density, excellent optical quality, compact size, and low electrical power consumption. [1] [2] [3]

The dynamic performance of MEMS deformable mirrors is commonly characterized using the transient response of a single actuator following a step command. Although this measurement provides a convenient reference for comparing devices, it represents only one deformation mode of a continuous mechanical structure. During adaptive optics operation, however, the mirror continuously generates wavefront corrections containing both low- and high-order spatial features. These corrections produce deformation patterns that differ substantially from an isolated actuator displacement and therefore may exhibit different transient behavior. [1] [4]

The objective of this work is to investigate how the transient response of a continuous-facesheet 3.5-μm stroke MEMS deformable mirror varies for a representative family of commanded deformation modes. The measurements include the conventional single-actuator response together with a series of checkerboard wavefronts having progressively smaller checkerboard periods. Rather than evaluating response time alone, the complete transient response — including rise time, settling behavior, overshoot, and oscillation — is examined for each deformation mode.

[1] T. G. Bifano, "Adaptive imaging: MEMS deformable mirrors", Nature Photonic (2011)
[2] K. Van Gorkom et al., "Characterizing deformable mirrors for the MagAO-X instrument", SPIE / arXiv (2021)
[3] Wang, Y., Xu, H., Li, D. et al. Performance analysis of an adaptive optics system for free-space optics communication through atmospheric turbulence. Sci Rep 8, 1124 (2018).
[4] B. P. Wallace, P. J. Hampton, C. H. Bradley and R. Conan, "Evaluation of a MEMS deformable mirror for an adaptive optics test bench", Optics Express (2006)
"The complete Data set for all product families – Multi-3.5, Multi-3.5-Dash & Multi-5.5 can be found in Appendix A"

STRUCTURAL DYNAMICS AND AIRFLOW

A continuous-facesheet MEMS deformable mirror behaves as a distributed mechanical structure rather than an array of independent control points. Motion produced by one electrostatic actuator is mechanically coupled through the continuous facesheet to neighboring actuators, so different commanded mirror shapes produce different distributions of bending, curvature, and mechanical loading across the mirror.

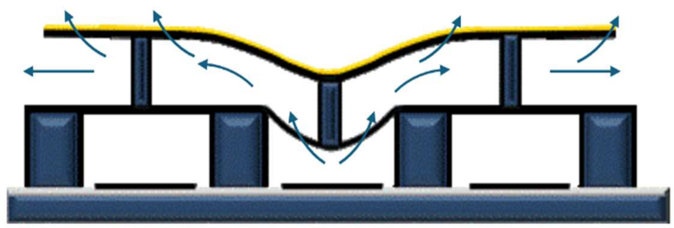

Figure 1. *Cross section of three actuators illustrating representative airflow paths around the perimeter, beneath the facesheet, and through mirror and actuator perforations.*

During operation, deformable mirrors generate complex surface figures that vary depending on the wavefront correction application. In systems designed to compensate for atmospheric turbulence, including astronomical imaging, free-space optical communications, directed-energy systems, and long-range imaging, the mirror continuously corrects rapidly changing wavefront distortions that contain irregular features spanning a broad range of spatial scales. In microscopy and other imaging applications, the dominant aberrations often arise from the optical system or the specimen itself and can frequently be represented by a superposition of low- and intermediate-order Zernike modes. Although these applications produce different classes of wavefront corrections, both require many actuators to move simultaneously, often with neighboring actuators undergoing different displacements. As a result, the transient response of the mirror reflects the combined effects of structural coupling within the continuous facesheet and airflow through the MEMS microstructure.

The checkerboard deformation modes investigated in this work are not intended to reproduce atmospheric turbulence or Zernike-based aberrations directly. Instead, they provide a systematic family of well-defined deformation modes that exercise different patterns of actuator interaction while remaining simple, repeatable, and straightforward to analyze. This controlled set of test shapes provides a practical means of investigating how the transient response of the mirror depends on the geometry of the commanded surface figure.

The air surrounding the actuator structure also influences the transient response. As the mirror moves toward or away from the substrate, the volume beneath the facesheet changes and the trapped air must rapidly redistribute. Air can flow around the perimeter of the mirror, beneath the facesheet, and through perforations in the mirror and electrostatic actuator (not shown in this cross section). If these airflow paths restrict the movement of the air, pressure develops beneath the moving mirror and resists its motion. This phenomenon, known as squeeze-film damping, has been shown in numerous MEMS studies to significantly influence the transient response of electrostatically actuated MEMS devices operating at atmospheric pressure.

The relevant damping mechanisms—including viscous resistance associated with airflow through confined MEMS geometries and the elastic (spring-like) response of enclosed air when its motion is highly constrained—have been comprehensively reviewed by Bao and Yang [5] and provide a useful qualitative framework for interpreting the experimental observations presented in this work.

The transient response of a continuous-facesheet MEMS deformable mirror is therefore governed by the combined effects of structural dynamics and airflow within the MEMS microstructure. The present work does not attempt to separate these mechanisms experimentally. Instead, it characterizes the overall dynamic response of the mirror for a series of representative deformation modes and discusses the observations within the context of the published MEMS damping literature.

[5] Bao, M., and Yang, H., "Squeeze film air damping in MEMS," Sensors and Actuators A: Physical, 136(1), 3–27 (2007).

EXPERIMENTAL METHODOLOGY

The dynamic response of the deformable mirror was evaluated using the family of commanded deformation modes shown in Figure 2. The command set consists of the conventional single-actuator displacement together with checkerboard patterns having progressively smaller checkerboard periods (6×6, 4×4, 3×3, 2×2, and 1×1). These deformation modes provide systematic progression from a localized actuator displacement to increasingly fine periodic mirror shapes while maintaining a repeatable command geometry.

The single-actuator command represents the conventional dynamic characterization used throughout the deformable mirror community and provides a useful baseline for comparison. The checkerboard patterns extend this characterization by requiring coordinated motion of many actuators across the mirror aperture. As the checkerboard period decreases, neighboring actuator groups are increasingly required to move in opposite directions, producing progressively finer deformation patterns across the continuous facesheet.

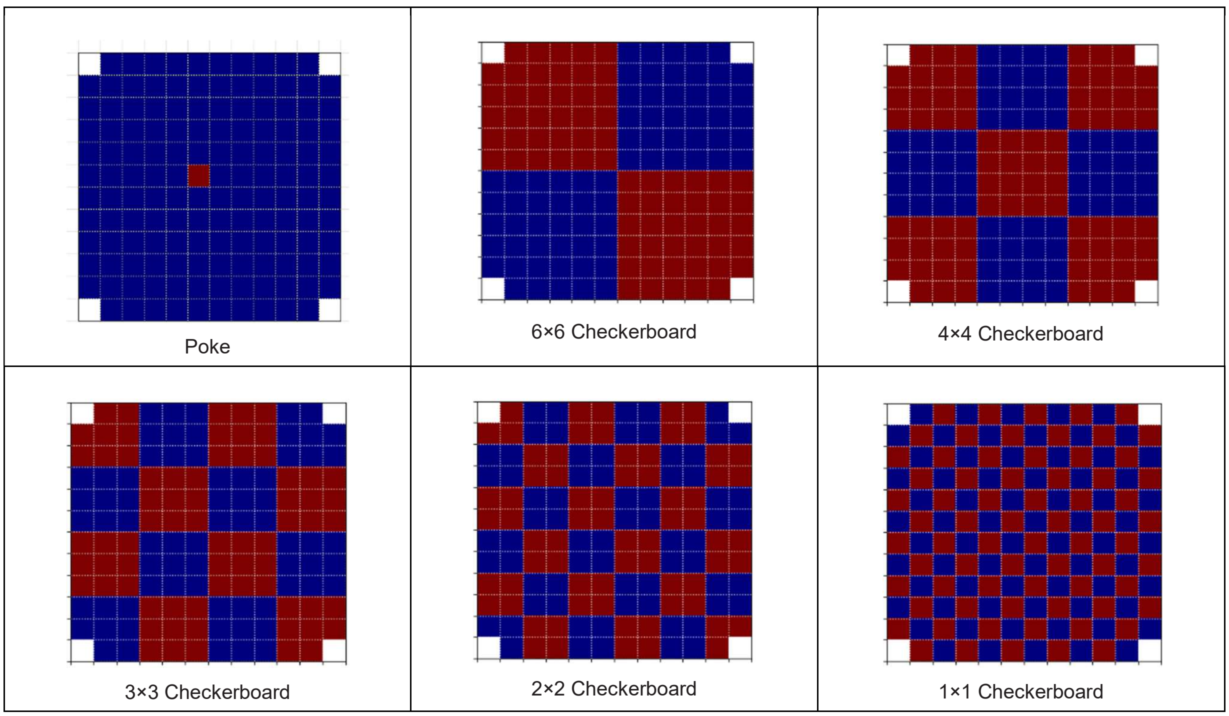

Figure 2. *Representative deformation modes used for dynamic characterization, including a single-actuator command and checkerboard patterns of progressively smaller spatial period.*

Dynamic measurements were performed using a custom high-speed time-resolved stroboscopic 3D surface profiler that measures the complete mirror surface following a commanded step input. The transient surface was measured at successive time delays following the applied command, allowing the temporal evolution of the entire mirror surface to be reconstructed.

Unlike conventional Laser Doppler Vibrometer (LDV) measurements, which can be used to measure the displacement of a single point on the mirror surface, the optical profiler provides the complete surface figure at each point in time. This enables both a direct comparison with conventional single-point measurements and the calculation of the transient response of the entire optical surface.

For each commanded deformation mode, the steady-state surface figure was first measured after the mirror had fully settled. This surface served as the reference wavefront. At each subsequent time step during the transient measurement, the instantaneous surface was compared with this reference, and the root-mean-square (RMS) surface error was calculated over the optical aperture. The resulting RMS response provides a direct measure of how rapidly the entire mirror converges to the desired wavefront.

Figure 3 compares the response obtained using a conventional LDV measurement with measurements obtained using the stroboscopic optical profiler. The blue and orange curves represent the displacement measured at a single point using the LDV and optical profiler, respectively, demonstrating excellent agreement between the two techniques. Both measurements indicate a response time of approximately 114 μs for the center of the actuated mirror segment.

The green curve shows the RMS surface error measured over the optical aperture. Although the center actuator reaches its commanded displacement in approximately 114 μs, the RMS response indicates that neighboring regions of the continuous facesheet require additional time to converge to the final wavefront, resulting in an overall response time of approximately 160 μs. This difference illustrates that the response of an individual actuator does not fully describe the transient behavior of the complete optical surface.

For adaptive optics applications, the quality of the corrected wavefront depends on the entire mirror surface rather than the displacement of a single actuator. Consequently, RMS surface error was selected as the primary response metric throughout this study. This approach provides a more representative measure of mirror dynamics for the checkerboard deformation modes investigated in the following sections.

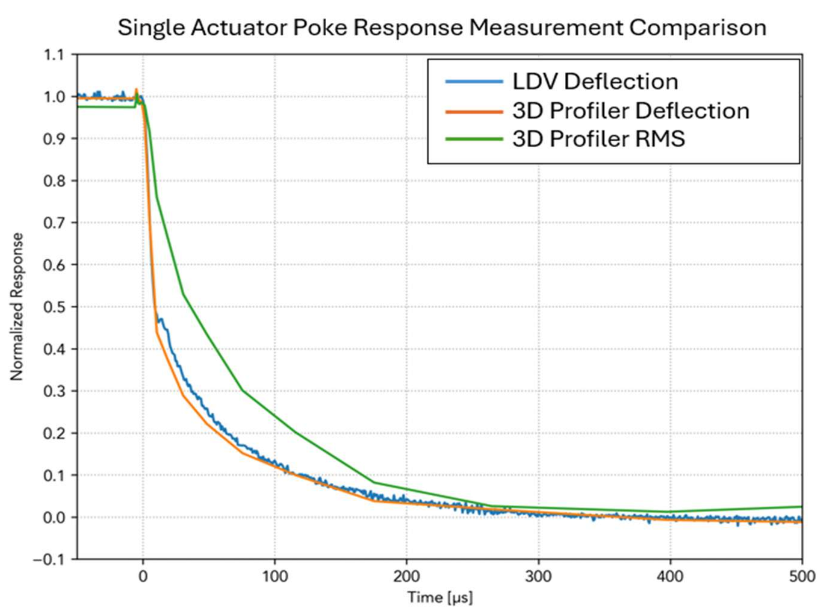

Figure 3. *Comparison of conventional single-point dynamic measurements using a laser Doppler vibrometer (LDV) and a stroboscopic 3D optical profiler. While both techniques produce nearly identical response times at the center of the actuated mirror actuator, the RMS surface error calculated from the full mirror surface demonstrates that the surrounding facesheet continues to settle after the center of the actuator has reached its commanded position.*

EXPERIMENTAL RESULTS

The transient response of the continuous-facesheet MEMS deformable mirror was evaluated using the family of deformation modes shown in Figure 2. Measurements were performed for commanded surface displacements of 150 nm, 750 nm, and 1500 nm. Figures 4 through 6 present the normalized RMS surface response for each deformation mode at the three command amplitudes, and Table 1 summarizes the measured RMS response times.

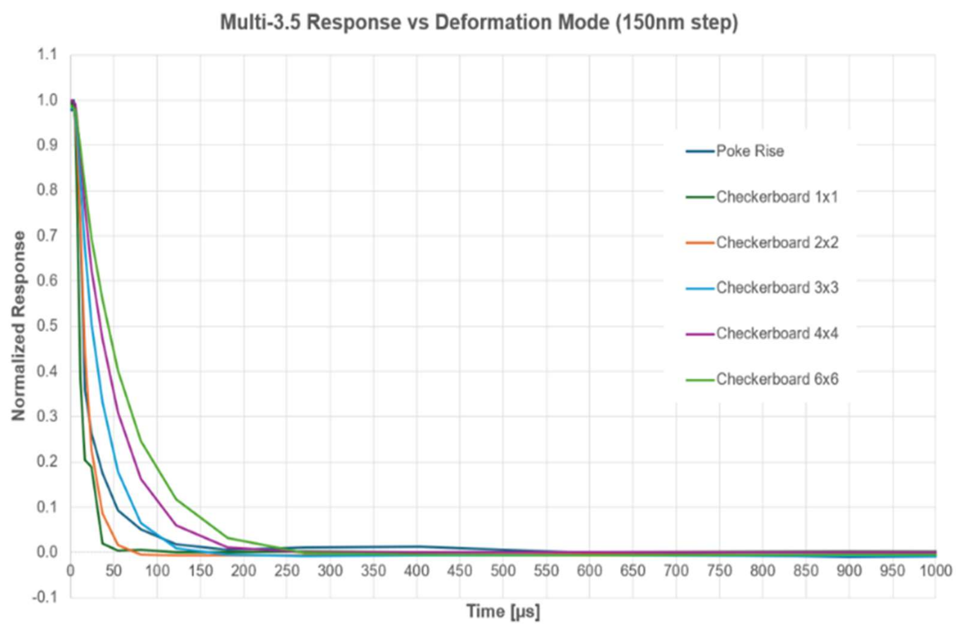

Figure 4. *Normalized RMS transient response for a 150 nm commanded surface displacement.*

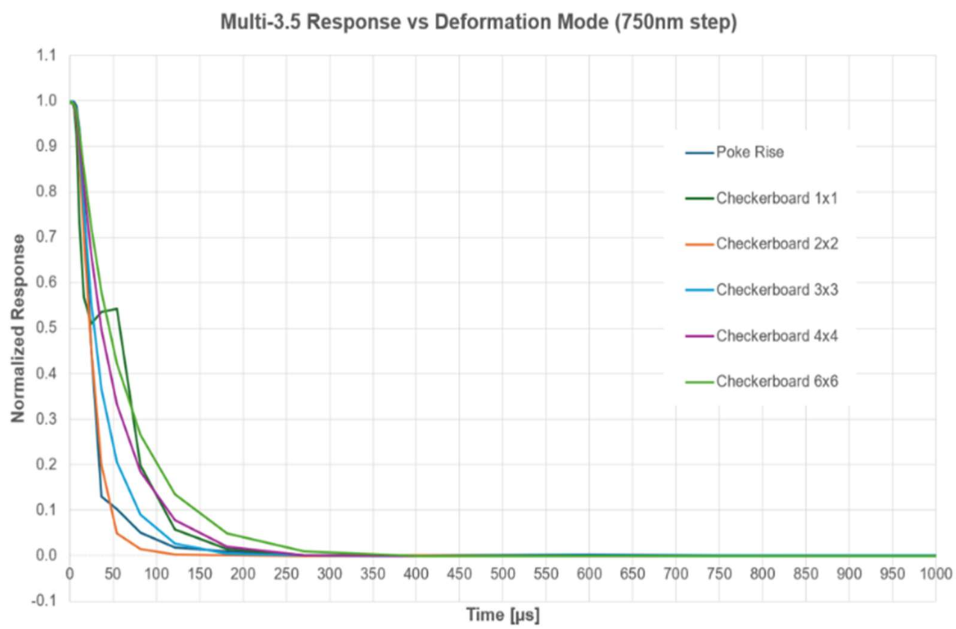

Figure 5. *Normalized RMS transient response for a 750 nm commanded surface displacement.*

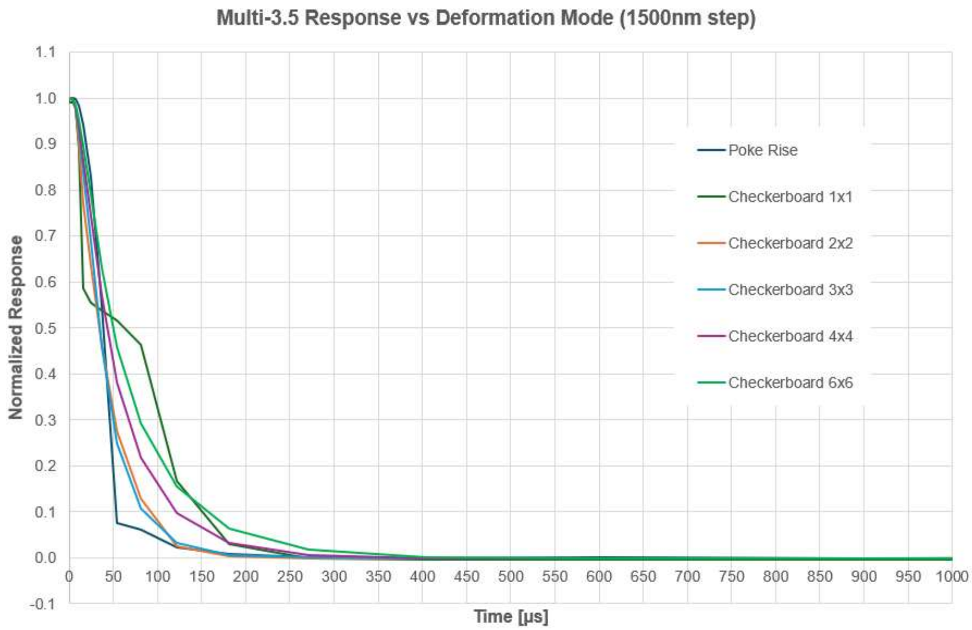

Figure 6. *Normalized RMS transient response for a 1500 nm commanded surface displacement.*

Table 1. Measured response time (time for RMS surface error to decay from 90% to 10%) for each deformation mode and command amplitude, baseline Multi-3.5 DM.

Mirror Deformation Mode	90%–10% RMS Error Decay Time (µs) of baseline Multi-3.5 DM		
	150 nm step	750 nm step	1500 nm step
Poke	46	47	44
1×1 Checkerboard	25	102	140
2×2 Checkerboard	28	39	81
3×3 Checkerboard	65	68	73
4×4 Checkerboard	96	102	107
6×6 Checkerboard	123	133	142

Several trends are immediately apparent from the measured responses. First, the deformation mode has a pronounced influence on the transient response of the mirror. The conventional single-actuator response provides an RMS response time of approximately 44 to 47 µs over the range of command amplitudes investigated. The checkerboard deformation modes, however, exhibit substantially different behavior.

On average, the 2×2 checkerboard exhibits the fastest response of all deformation modes measured, with RMS response times ranging from 28 µs for the 150 nm step to 81 µs for the 1500 nm step. The 3×3 checkerboard produces response times of approximately 65 to 73 µs, while the 4×4 checkerboard settles considerably more slowly, requiring approximately 96 to 107 µs. The slowest response is observed for the 6×6 checkerboard, with response times between 123 and 142 µs.

These measurements demonstrate that the transient response cannot be adequately characterized by a single response time that is independent of the commanded mirror shape. Instead, the response depends strongly on the deformation mode applied to the continuous facesheet.

A second important observation is that the response time is most strongly influenced by the deformation mode, with a smaller influence from the step size. Increasing the commanded displacement by a factor of ten, from 150 nm to 1500 nm, produces comparatively small changes in response time for most deformation modes. For example, the poke response changes by less than 7%, while the 4×4 and 6×6 checkerboards increase by only approximately 11 to 16%. The largest amplitude dependence is observed for the 1×1 and 2×2 checkerboards, although even here the variation is smaller than the differences observed between deformation modes.

The transient response curves also reveal differences in the overall shape of the response. The poke, 2×2, 3×3, and 4×4 deformation modes exhibit predominantly monotonic settling. The finest checkerboard, however, exhibits a modest amount of overshoot and low-amplitude oscillation before converging to the final wavefront for the larger command amplitudes. Although the oscillations are relatively small, they indicate that the effective damping of the mirror changes with deformation mode. The 1×1 checkerboard also exhibits a response time that is considerably more sensitive to command amplitude than any other deformation mode tested, in contrast to the comparatively weak amplitude dependence observed elsewhere. This behavior is consistent with operation nearer an elastic-dominated damping regime, in which the response depends more strongly on the degree of air compression than on flow velocity alone, though a full accounting of this effect is left for future work.

"The complete Data set for all product families – Multi-3.5, Multi-3.5-Dash & Multi-5.5 can be found in Appendix A"

DISCUSSION

The experimental results demonstrate that the dynamic response of a continuous-facesheet MEMS deformable mirror depends strongly on the commanded deformation mode. This observation is consistent with the physical behavior of a distributed mechanical structure in which both the continuous facesheet and the surrounding air influence the transient response.

The continuous facesheet mechanically couples adjacent actuators, so each deformation mode produces a different distribution of bending and curvature across the mirror. At the same time, movement of the facesheet redistributes the air trapped beneath the mirror. Air must flow around the mirror perimeter, beneath the facesheet, and through perforations in the mirror and electrostatic actuator. The resistance to this airflow produces squeeze-film damping, which has been identified in the MEMS literature as a significant contributor to the transient response of electrostatically actuated structures operating in air.

The present measurements do not independently separate these two mechanisms. Instead, they characterize the combined effects on the transient response of the complete deformable mirror. The measured differences between deformation modes therefore reflect changes in the combined structural and airflow dynamics associated with each commanded mirror shape.

One significant observation is that the deformation mode has a greater influence on response time than command amplitude. Across the range of amplitudes investigated, the measured response times vary only modestly, whereas changing the deformation mode alters the response time by more than a factor of three. This suggests that, for continuous-facesheet MEMS deformable mirrors operating within their normal linear range, the geometry of the commanded wavefront is a more important determinant of transient response than the magnitude of the commanded displacement.

The results also illustrate that conventional single-actuator characterization provides only a partial description of mirror dynamics. The poke response falls approximately in the middle of the range of measured response times and therefore does not represent either the fastest or the slowest behavior of the mirror. Consequently, a single response-time specification cannot fully describe the transient performance of the device under the variety of wavefronts encountered during adaptive optics operation.

The checkerboard methodology presented here provides a practical framework for extending dynamic characterization beyond conventional single-point measurements. By evaluating a family of representative deformation modes, the methodology provides a more complete description of mirror behavior while remaining straightforward to implement using standard interferometric measurement techniques.

APPENDIX (A)

The following data shows the transient response of product families Multi-3.5, Multi-3.5-Dash DM and Multi-5.5 DM using the set of deformation modes shown in Figure 2. Measurements were performed for commanded surface displacements of 150 nm, 750 nm, and 1500 nm.

Product Family — Multi-3.5 DM

Figures 7 through 9 present the normalized RMS surface response of Multi-3.5 DM for each deformation mode at the three command amplitudes, and Table 2 summarizes the measured RMS response times.

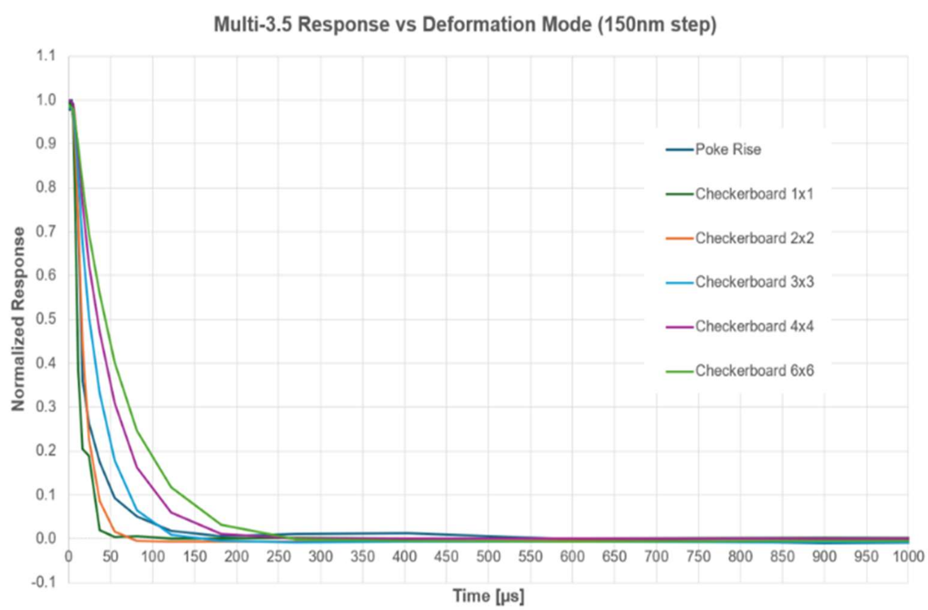

Figure 7. *Normalized RMS transient response for a 150 nm commanded surface displacement.*

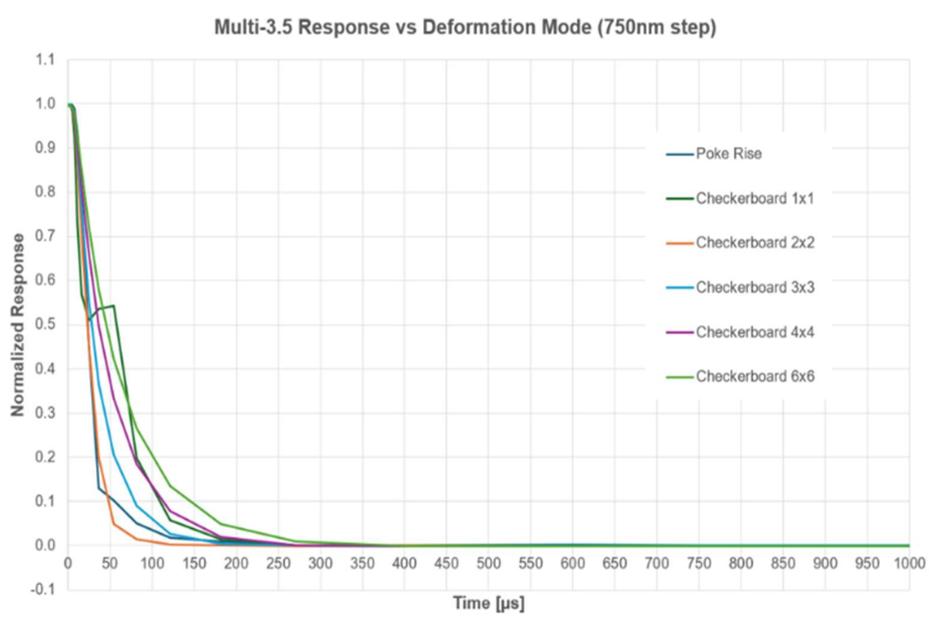

Figure 8. *Normalized RMS transient response for a 750 nm commanded surface displacement.*

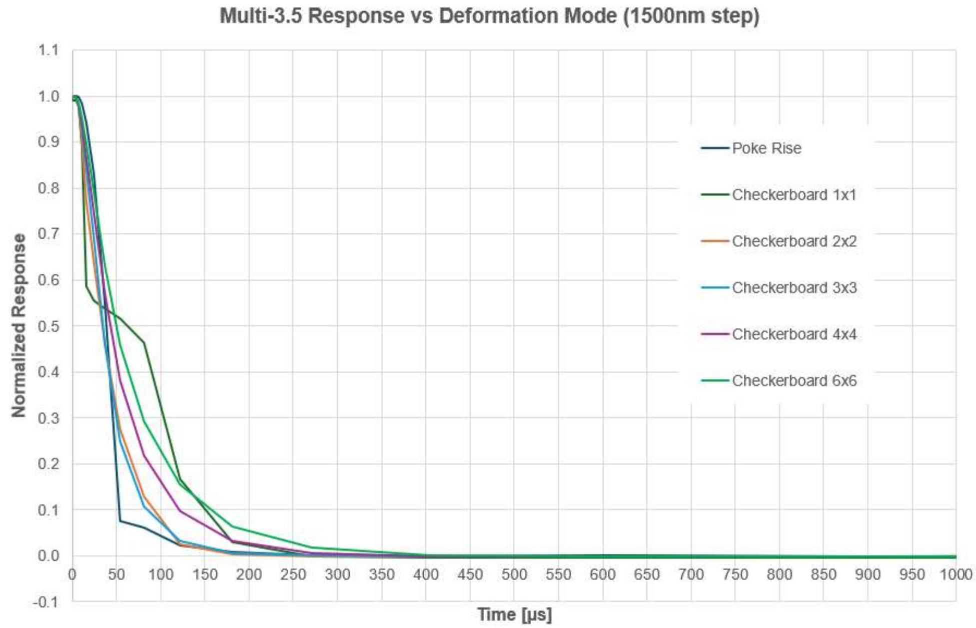

Figure 9. *Normalized RMS transient response for a 1500 nm commanded surface displacement.*

Table 2. Measured response time (time for RMS surface error to decay from 90% to 10%) for each deformation mode and command amplitude, baseline Multi-3.5 DM.

Mirror Deformation Mode	90%–10% RMS Error Decay Time (µs) of baseline Multi-3.5 DM		
	150 nm step	750 nm step	1500 nm step
Poke	46	47	44
1×1 Checkerboard	25	102	140
2×2 Checkerboard	28	39	81
3×3 Checkerboard	65	68	73
4×4 Checkerboard	96	102	107
6×6 Checkerboard	123	133	142

Product Family — Multi-3.5-Dash DM

Figures 10 through 12 present the normalized RMS surface response of Multi-3.5-Dash DM for each deformation mode at the three command amplitudes, and Table 3 summarizes the measured RMS response times.

Figure 10. *Normalized RMS transient response for a 150 nm commanded surface displacement (Multi-3.5-Dash DM).*

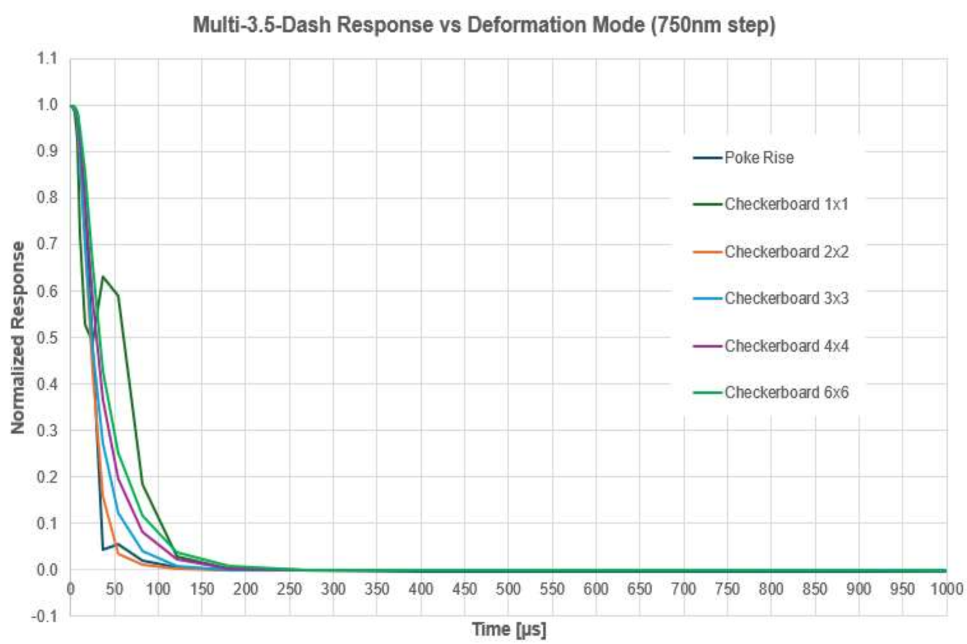

Figure 11. *Normalized RMS transient response for a 750 nm commanded surface displacement (Multi-3.5-Dash DM).*

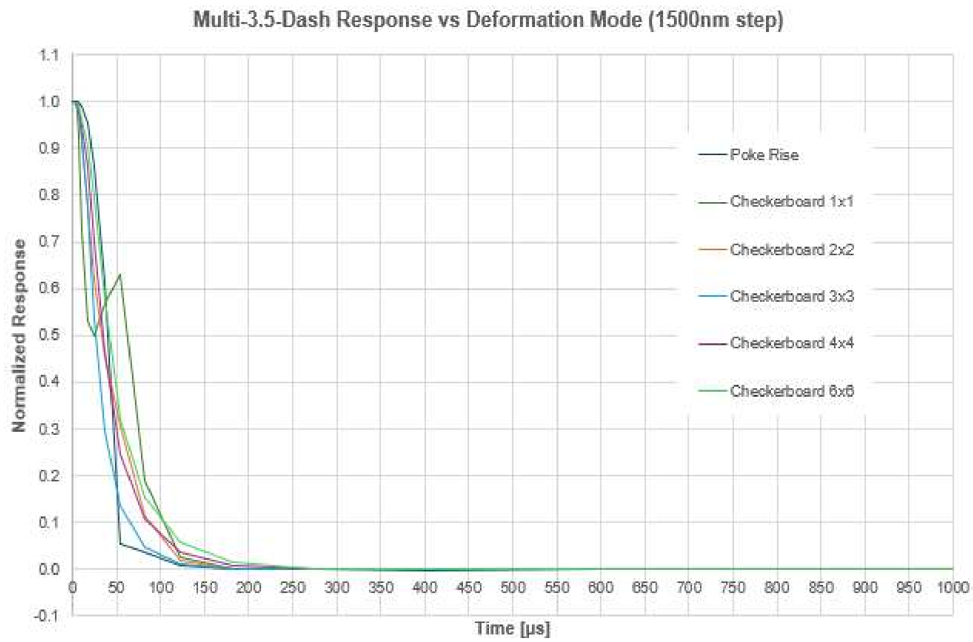

Figure 12. *Normalized RMS transient response for a 1500 nm commanded surface displacement (Multi-3.5-Dash DM).*

Table 3. Measured response time (time for RMS surface error to decay from 90% to 10%) for each deformation mode and command amplitude, baseline Multi-3.5-Dash DM.

Mirror Deformation Mode	90%–10% RMS Error Decay Time (µs) of baseline Multi-3.5-Dash DM		
	150 nm step	750 nm step	1500 nm step
Poke	34	31	36
1×1 Checkerboard	18	95	96
2×2 Checkerboard	25	35	76
3×3 Checkerboard	49	51	53
4×4 Checkerboard	63	65	72
6×6 Checkerboard	73	76	87

Product Family — Multi-5.5 DM

Figures 13 through 15 present the normalized RMS surface response of Multi-5.5 DM for each deformation mode at the three command amplitudes, and Table 4 summarizes the measured RMS response times.

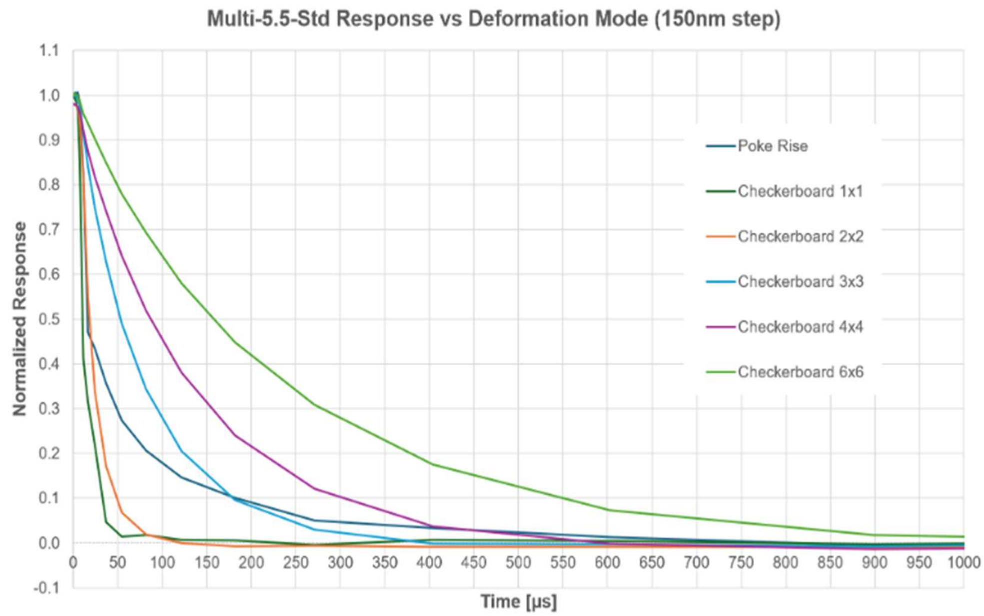

Figure 13. *Normalized RMS transient response for a 150 nm commanded surface displacement (Multi-5.5 DM).*

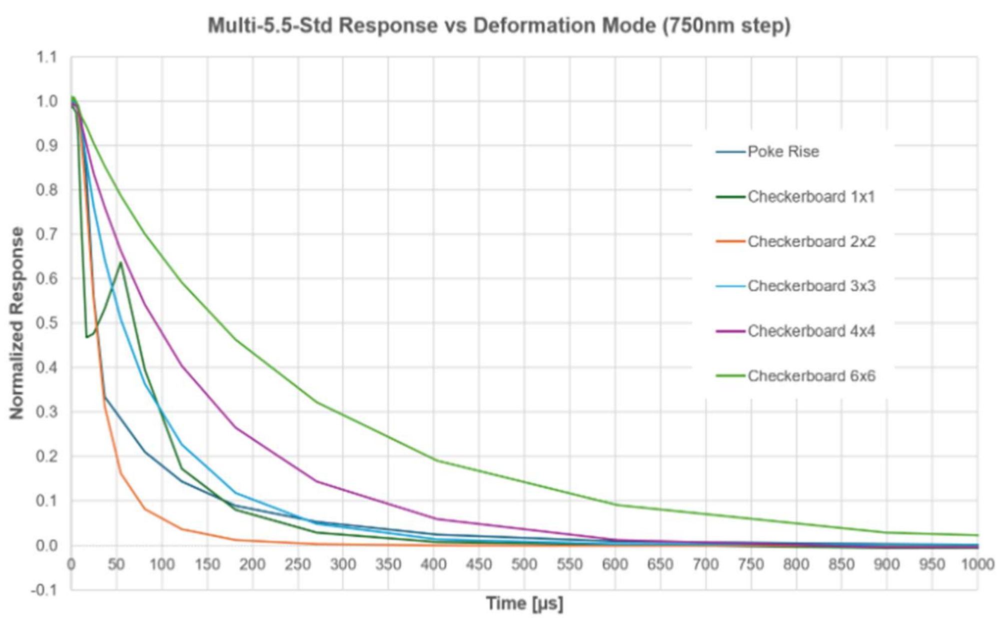

Figure 14. *Normalized RMS transient response for a 750 nm commanded surface displacement (Multi-5.5 DM).*

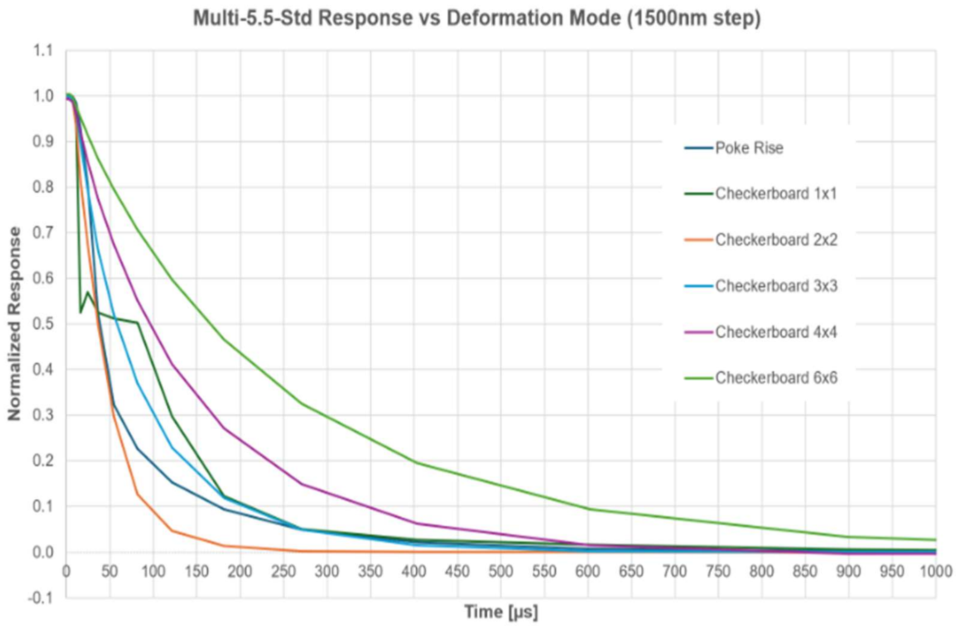

Figure 15. *Normalized RMS transient response for a 1500 nm commanded surface displacement (Multi-5.5 DM).*

Table 4. Measured response time (time for RMS surface error to decay from 90% to 10%) for each deformation mode and command amplitude, baseline Multi-5.5 DM.

Mirror Deformation Mode	90%–10% RMS Error Decay Time (µs) of baseline Multi-5.5 DM		
	150 nm step	750 nm step	1500 nm step
Poke	166	162	163
1×1 Checkerboard	26	160	199
2×2 Checkerboard	41	65	82
3×3 Checkerboard	167	190	189
4×4 Checkerboard	290	322	327
6×6 Checkerboard	524	558	562

Measured Response Time Comparison

Tables 5 through 7 and Figures 16 through 18 compare the measured response time (time for RMS surface error to decay from 90% to 10%) for each deformation mode and command amplitude, across the Multi-3.5 DM, Multi-3.5-Dash DM, and Multi-5.5 DM product families.

Table 5. Measured response time for each deformation mode and product family at 150 nm command amplitude.

Mirror Deformation Mode	90%–10% RMS Error Decay Time (µs) of 150 nm command amplitude		
	Multi-3.5 DM	Multi-3.5 Dash DM	Multi-5.5 DM
Poke	46	34	166
1×1 Checkerboard	25	18	26
2×2 Checkerboard	28	25	41
3×3 Checkerboard	65	49	167
4×4 Checkerboard	96	63	290
6×6 Checkerboard	123	73	524

Figure 16. *Comparison of measured response time across product families for a 150 nm commanded surface displacement.*

Table 6. Measured response time for each deformation mode and product family at 750 nm command amplitude.

Mirror Deformation Mode	90%–10% RMS Error Decay Time (µs) of 750 nm command amplitude		
	Multi-3.5 DM	Multi-3.5-Dash DM	Multi-5.5 DM
Poke	47	31	162
1×1 Checkerboard	102	95	160
2×2 Checkerboard	39	35	65
3×3 Checkerboard	68	51	190
4×4 Checkerboard	102	65	322
6×6 Checkerboard	133	76	558

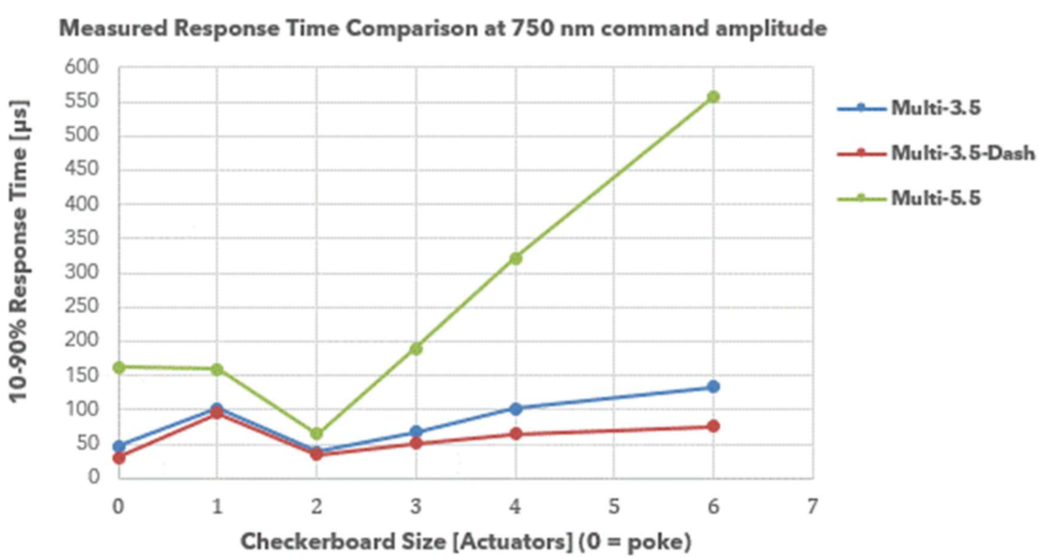

Figure 17. *Comparison of measured response time across product families for a 750 nm commanded surface displacement.*

Table 7. Measured response time for each deformation mode and product family at 1500 nm command amplitude.

Mirror Deformation Mode	90%–10% RMS Error Decay Time (µs) of 1500 nm command amplitude		
	Multi-3.5 DM	Multi-3.5-Dash DM	Multi-5.5 DM
Poke	44	36	163
1×1 Checkerboard	140	96	199
2×2 Checkerboard	81	76	82
3×3 Checkerboard	73	53	189
4×4 Checkerboard	107	72	327
6×6 Checkerboard	142	87	562

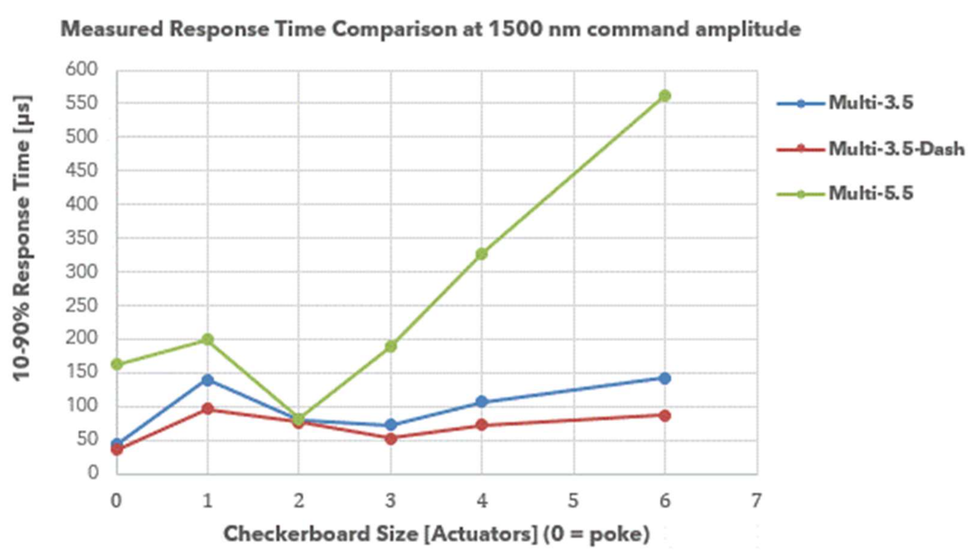

Figure 18. *Comparison of measured response time across product families for a 1500 nm commanded surface displacement.*

APPLICATIONS

The results presented in this work have direct implications for adaptive optics control system design in free-space laser communications, directed-energy systems, and astronomical imaging, where atmospheric turbulence must be corrected in real time at high update rates. In these applications, achievable closed-loop bandwidth is limited by how quickly the deformable mirror responds to a newly commanded wavefront; because turbulence continuously combines low- and high-order spatial features rather than isolated actuator motions, a conventional single-actuator step response is an incomplete predictor of the mirror's true achievable bandwidth. The specific response times reported here are specific to the mirror configurations and test conditions used in this study and are not intended to predict settling times for other systems or applications. Rather, the checkerboard command set was chosen to conveniently span a range of spatial frequencies, demonstrating that transient response varies meaningfully with the spatial content of the commanded wavefront.

This is the key consideration for optimizing an AO control algorithm: controller gains, latency budgets, and predictive control strategies should be matched to how settling time changes across the spatial frequencies that an application is expected to command, rather than to a single generic specification. This distinction is especially important for high-bandwidth applications such as free-space laser communications and directed-energy beam control, where beam quality is highly sensitive to residual wavefront error, and for extreme adaptive optics systems in astronomical imaging, where fast convergence is required to preserve contrast and resolution.